Electronic Supplementary Material (ESI) for Physical Chemistry Chemical Physics.
This journal is © the Owner Societies 2020

Supplementary Information for

Collaboration between Pt-dimer and neighboring Co-Pd Atoms Triggers Efficiency Pathways for Oxygen Reduction Reaction

Haolin Li,[a,b] Sheng Dai,[d] Dinesh Bhalothia,[b] Jyh-Pin Chou,[e] Alice Hu[a,f*] and Tsan-Yao Chen[b,c,g*]*

a. Department of Mechanical Engineering, City University of Hong Kong, Hong Kong, China

b. Department of Engineering and System Science, National Tsing Hua University, Hsinchu, Taiwan

c. Institute of Nuclear Engineering and Science, National Tsing Hua University, Hsinchu, Taiwan

d. School of Chemistry & Molecular Engineering, East China University of Science and Technology, Shanghai 200237, P.R. China

e. Department of Physics, National Changhua University of Education, Changhua, Taiwan

f. Department of Materials Science and Engineering, City University of Hong Kong, Hong Kong, China

g. Department of Materials Science and Engineering, National Taiwan University of Science and Technology, Taipei 10617, Taiwan

[*]**Co-corresponding author**: (T.-Y. C) Email: chencaeser@gmail.com / tsanyao@mx.nthu.edu.tw; (J.-P. C) Email: jpchou@cc.ncue.edu.tw; (A. H) Email: alicehu@cityu.edu.hk;

Note S1 | The selection of stable adsorption sites of chemisorbed O_2, O^{ads}, H_2O and OH^- for all model catalysts.

Generally, it is believed that the most stable chemisorption configuration is two-fold bridge site (i.e. M-b site) for O_2 molecule, three-fold hollow sites (i.e. M-h / f site, where h and f stand respectively for the hcp and fcc sites) for atomic O^{ads}, top site (i.e. M-t site) for H_2O molecule, and top / bridge site (i.e. M-t / M-b site) for OH^- radicals on a catalyst surface; where "M" is Pd or Pt atoms in this study. Fig. S2. displayed the atomic adsorption configurations of the reactants (O_2 and H_2O), the intermediate (O^{ads}) and the product (OH^-) at different adsorption sites on the representative model catalysts (Pd, Pt_0, Pt_2, Pt_{16}, Pt_{32}, Pt), the corresponding E_{ads} of the four ORR-species are listed in Table S1.

Note S2 | Discussion of hcp and fcc hollow sites for O^{ads} on transition metals.

It is generally believed that the (111) facet of a transition metal presents a staggered distribution of two hollow sites with differentiated adsorption energy for O^{ads} (E_{ads}-O^{ads}), i.e., the E_{ads}-O^{ads} of three-fold fcc (M-f) is weaker than that of three-fold hcp (M-h) sites. Take the Pt (111) model as an example, the fcc site with a relatively strong E_{ads}-O^{ads} (Pt_3-f, −1.29 eV) on the Pt surface is considered to be in favor of the O-O bond breakage and the counterpart weak hcp site (Pt_3-h, −0.88 eV) is more suitable for the subsequent O^{ads} reduction (see Table S1). Ideally, after the O_2^{ads} dissociation, half of O^{ads} will be relocated to the weak hcp site and the rest of O^{ads} will be trapped at the strong fcc site. Then, the O^{ads} will be quickly formed a OH^- and release the hcp sorption site. Meanwhile, some of the O^{ads} are held by a stronger E_{ads}-O^{ads} in fcc sites, therefore, delay the subsequent hydration reaction. As ORR continues, with the uneven redox kinetics by the variation of E_{ads}-O^{ads}, a growing number of the fcc sites is poisoned by O^{ads} which eventually leads to passivation of the surface in a pure metal model. Therefore, the hcp hollow site with relatively weak E_{ads}-O^{ads} is expected to exhibit a better O^{ads} reduction capability than that of fcc hollow site in a transition metal surface.

Besides, the E_{ads}-O^{ads} discrepancy (ΔE_{ads}-O^{ads}) between the two types of the hollow site has an impact on ORR performance. To be specific, with a relatively weak E_{ads}-O^{ads} and a lower ΔE_{ads}-O^{ads}, the two O^{ads} between adjacent hcp and fcc sites would tend to recombine into O_2^{ads} as a result obstructs the O_2 dissociation. On the contrary, a large ΔE_{ads}-O^{ads} results in out-of-step O^{ads} hydration between the two reaction sites. As compared to that of M-h sites, a lower hydration reaction rate is expected due to the higher barrier to break the O^{ads} bond from the M-f sites thus suppressing the ORR efficiency of entire surface. Therefore, the moderate E_{ads}-O^{ads}, rational ΔE_{ads}-O^{ads} and the adsorption sites with varies

intermediates selectivity are essential criteria for developing high-performance metallic catalysts in ORR

Note S3 | Details about the stable initial-state (IS), transition-state (TS) and final-state (FS) geometries of the "O_2 dissociation" and "O^{ads} hydration" steps on the Pt_2 model surface.

In the first step the "O_2 dissociation", the chosen initial-state (IS) and final-state (FS) geometries are respectively an O_2 molecule adsorbing on a diatomic bridge site and then being split into two atomic O^{ads} that relocate onto two adjacent hollow sites. In the second step "the O^{ads} hydration", the chosen IS and FS are one adsorbed O^{ads} atom on the hollow site interacting with a neighboring H_2O molecule adsorbed on a metal atom. The final product is two OH radicals. The transition-state (TS) structures (the highest NEB image) in the 1st and 2nd step reactions are respectively considered as the moments (i.e., the reaction energy barrier height) of O-O bond breakage and O-H bond formation.

In the Pt_2 model, the stable geometries for O_2 adsorption are set as the IS of the 1st step. They are bridge sties in the Pt-dimer (P_2-b) in center, the Pt-Pd (PtPd-b) in the interface, and the Pd atoms (Pd_2-b) in the outmost region. After splitting, the O^{ads} atoms will move to the two Pt_1Pd_2-h sites adjacent to Pt_2-b, a pair of a Pt_1Pd_2-h site and a Pd_3-h site next to PtPd-b, and two Pd_3-h sites around the Pd_2-b corresponding to the FS of the 1st step for the aforementioned three bridge sites. In the 2nd step, the H_2O molecules are adsorbed atop the Pd atoms (i.e., Pd_1-t sites) in the Pd region for the subsequent hydration reactions. Atomic structures of the three reaction pathways (i.e., Pt_2-b path, PtPd-b path, Pd_2-b path) on the Pt_2 model surface are displayed in Fig. S3.

Note S4 | Calculated atomic magnetic moment of core-shell models.

To reveal the coupling interactions between surface cluster, shell layer and core regime inside Co-Pd-Pt trimetallic system, and their possible influences on charge relocation of the Pt-cluster, we calculated the layer-averaged spin magnetic moment of the representative Pt_0, Pt_2 and Pt_{16} models in comparison with the magnetic moment of bulk Pt, Pd and Co: see Fig. S5 (the corresponding data are listed in Table S5 and S6).

For the Pt atoms of the ternary models, the Pt_2 exhibits the strongest magnetic moments of 0.32 μ_B in its 1^{th} layer, followed by 0.23 μ_B of the Pt_{16}. Both calculated magnetic moments for Pt atoms of the Pt_2 and the Pt_{16} are conspicuously higher than that of bulk Pt (0.0 μ_B), which is likely to be due to the coupling between doped Pt atoms, surrounding Pd atoms and deep Co atoms. However, for the Pd atoms in the upper three layers (1^{st} / 2^{nd} / 3^{rd} layers), the spin magnetic moments per layer of the core-shell Pt_0, Pt_2 and Pt_{16} models are very close (~ 0.30 μ_B) and of the same magnitude as that of our calculated bulk Pd (0.31 μ_B). Meanwhile, the average magnetic moment for the third Pd-layer (0.31 μ_B) and the fourth Co-layer (1.67 μ_B) in Pd-Co interface of the bimetallic Pt_0 are equal to that of the calculated bulk Pd (0.31 μ_B) and bulk Co (1.67 μ_B), respectively. Therefore, the Pd layer here can be considered as relatively spin-insensitive compared with the Pt layer and Co layer. In contrast, the average magnetic moments of the deepest three Co layers (4^{th} / 5^{th} / 6^{th} layers) of the ternary Pt_2 (1.80 / 1.67 / 1.40) is slight lower than that of the binary Pt_0 (1.81 / 1.68 / 1.42) while much higher than that of the ternary Pt_{16} (1.74 / 1.50 / 0.98). It implies that the Pt atoms embedded on the surface from full coverage to even dimer size interact with deep Co atoms. Hence, the coupling effect between topmost Pt atoms and deep Co atoms proves to exist in the presence of interlayer Pd atoms.

To measure the possible relationship between the potential Pt / Co coupling and the charge relocation of the ternary model surfaces, we compared the average atomic magnetic moment (the blue bars) and the average charge-gain (the purple bars) of Pt atoms in the first layer of the Pt_2, Pt_{16} and pure Pt models, see the bar graph in Fig. S6. Obviously from the pure Pt to Pt_{16} to Pt_2, the magnetic moment per Pt atom on the surface rise continuously from 0.01 to 0.23 and then to 0.32 μ_B. Consistently, the charge-gain per Pt atom on the surface shows a comparable tendency to the magnetic moment change, from 0.04 to 0.09 and then to 0.19 e^-. Hence, as the magnetic moment of Pt atoms increases due to the coupling effect, more charge are gathering around these Pt atoms, i.e., a high density of electron is extracted in the near-Fermi level of the Pt dimer, thus generating the potential gradients between Pt dimer and its peripheral regions (proposed in section 3.2). As a result, those potential gradients induce a local prominent electric field on Pt dimer that make itself a highly active center on the alloy surface, which alter the adsorption affinity to the reactants and intermediates of ORR, in turn, the catalytic performances. Whereas for the Pt-covered models (the pure Pt and Pt_{16}), the charge localization around surface Pt atoms is suppressed due to the dominance of Pt on their surfaces.

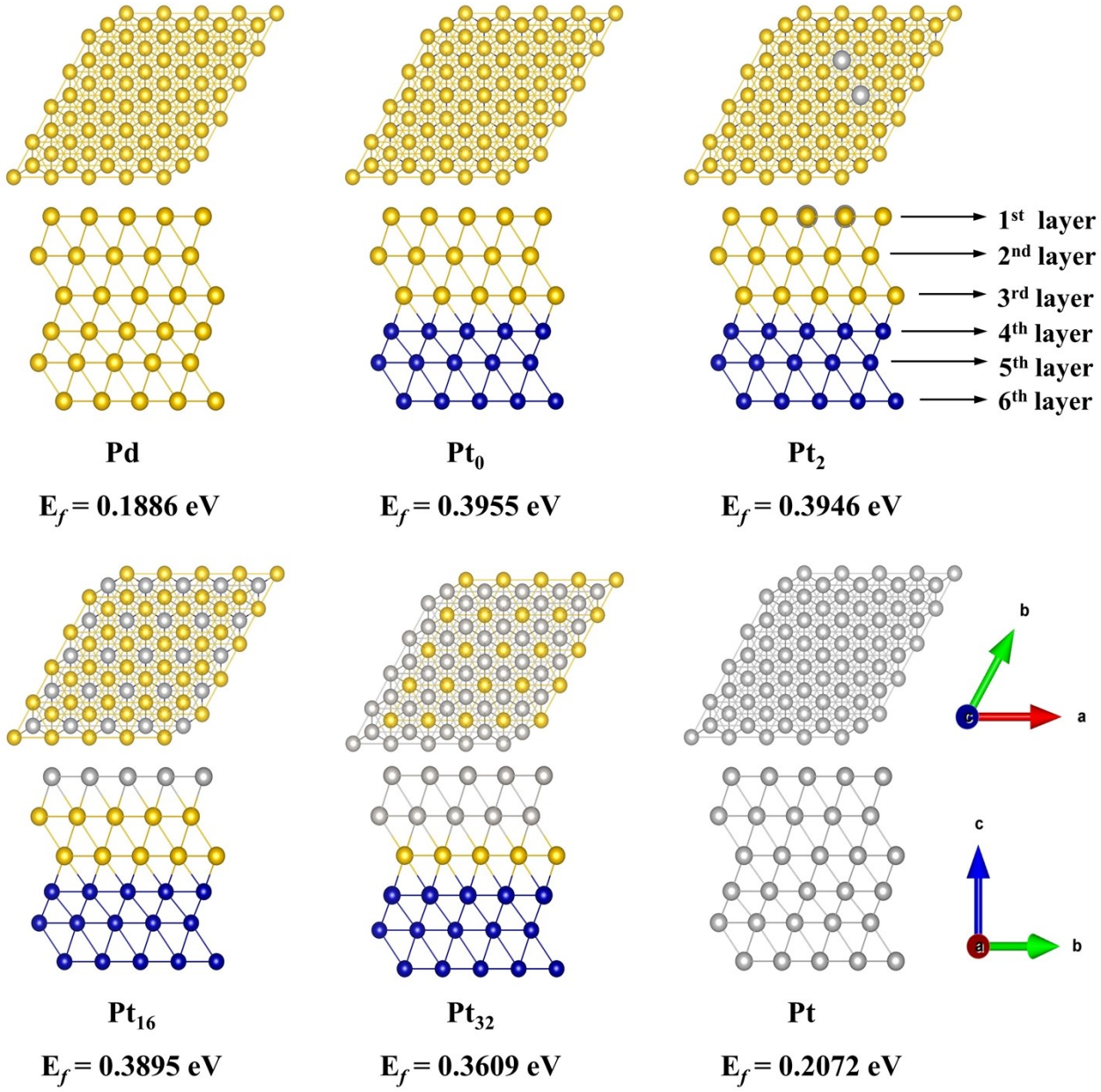

Fig. S1 | Top and side views of the pure Pd, the Co@Pd-Pt$_n$ (n = 0, 2, 16 and 32) and the pure Pt surface models. All the models are composed of six atomic layers with the first to third slabs as the shell layer and fourth to sixth slabs as the core component, together with the calculated E_f of each configuration. The grey, yellow and blue spheres represent Pt, Pd and Co atoms, respectively.

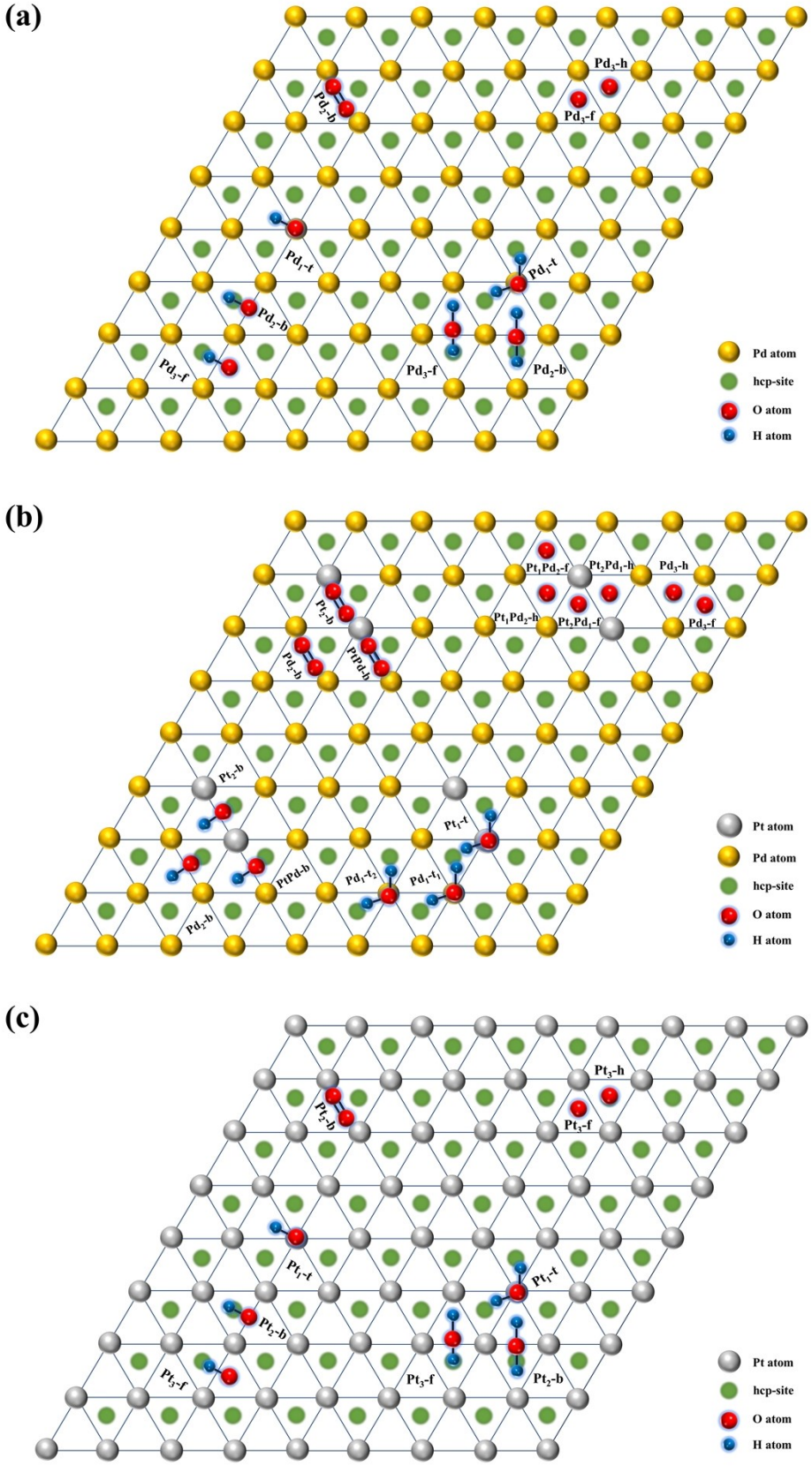
(a)
Pd3-h
Pd2-b
Pd3-f
Pd1-t
Pd1-t
Pd2-b
Pd3-f
Pd3-f
Pd2-b
Pd atom
hcp-site
O atom
H atom
(b)
Pt1Pd2-f
Pt2Pd1-h
Pd3-h
Pt2-b
Pt1Pd2-h
Pt2Pd1-f
Pd3-f
Pd2-b
PtPd-h
Pt2-b
Pt1-t
PtPd-b
Pd1-t2
Pd1-t1
Pd2-b
Pt atom
Pd atom
hcp-site
O atom
H atom
(c)
Pt3-h
Pt2-b
Pt3-f
Pt1-t
Pt1-t
Pt2-b
Pt3-f
Pt3-f
Pt2-b
Pt atom
hcp-site
O atom
H atom

Fig. S2 | Top views of the atomic adsorption structures of O_2, O^{ads}, H_2O and OH^- at different adsorption sites on (a) the pure Pd and Pd_0 models, (b) the Pt_2 model, (c) the Pt_{16}, Pt_{32} and pure Pt models. For clarity, only the top one-layer atoms of the models within four supercell surfaces are showed. The yellow, grey, red and blue balls stand for Pd, Pt, O and H atoms, respectively. The hollow sites on the surface above the green atoms and the vacancies correspond to the hcp sites and fcc sites, respectively.

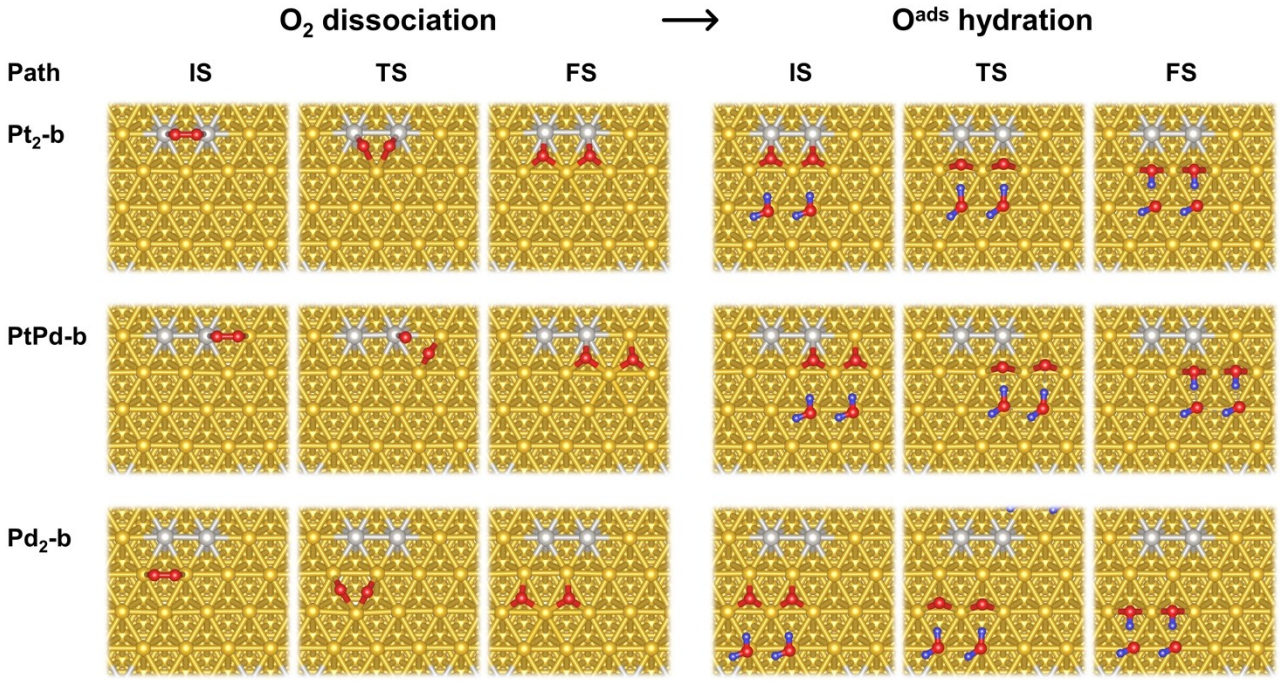

Fig. S3 | Top view structures of O_2 dissociation (1st step) and O^{ads} hydration (2nd step) of the three possible ORR paths on the Pt_2 surface model. The IS, TS and FS respectively stands for initial state, transition state and final state. The grey, yellow, red and blue spheres stand for Pt atoms, Pd atoms, O and H atoms, respectively.

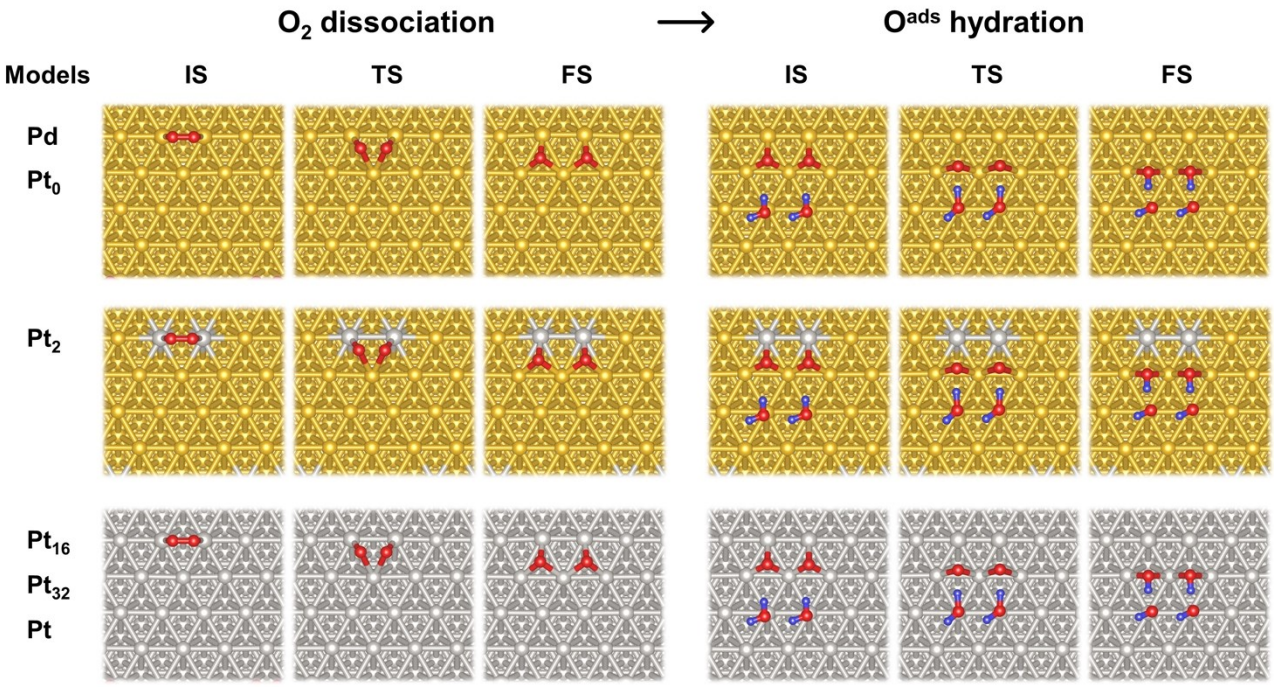

Fig. S4 | Top view structures of the selected O_2 dissociation and O^{ads} hydration stages on the pure Pd, Pt_0, Pt_{16}, Pt_{32} and pure Pt surface models. The IS, TS, and FS respectively stands for initial state, transition state and final state. The grey, yellow, red and blue spheres stand for Pt atoms, Pd atoms, O and H atoms, respectively.

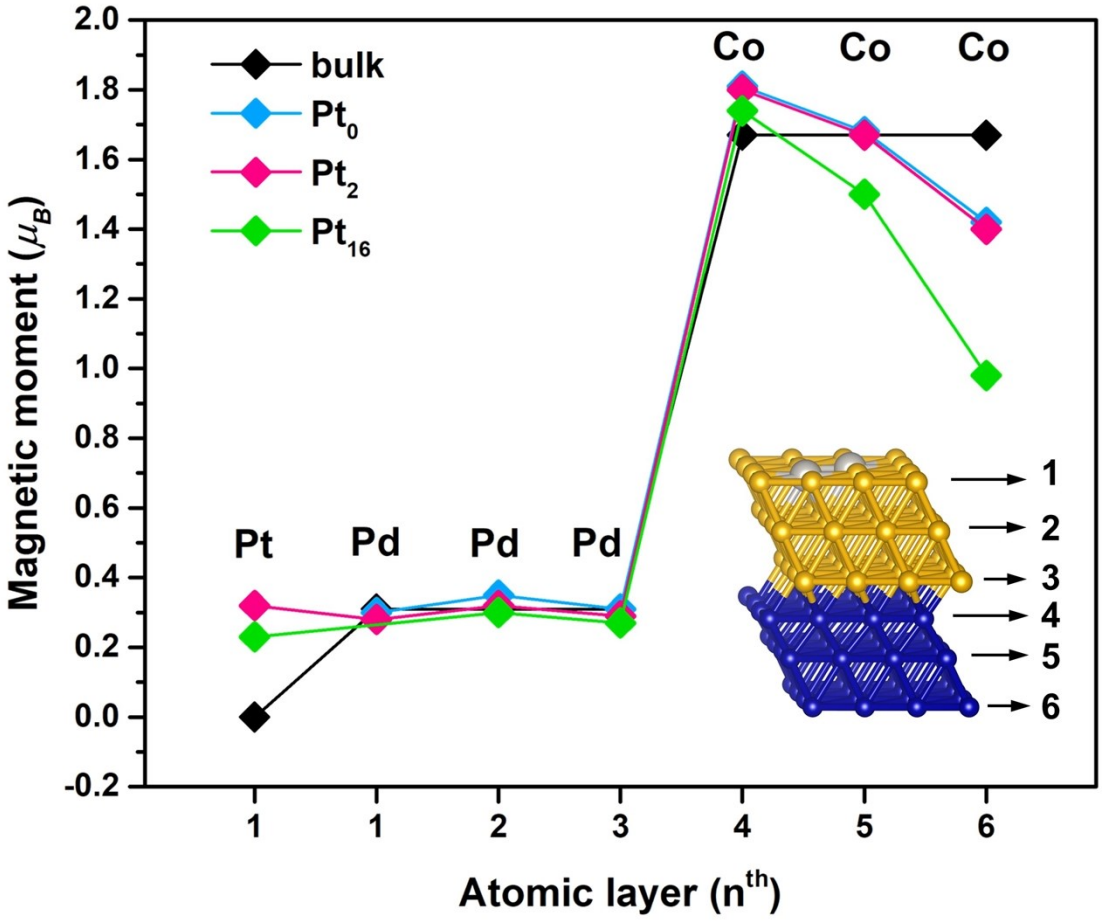

Fig. S5 | Calculated magnetization of different bulk and six-layer slab models. The black rhombi symbols denote the bulk magnetic moment of Pt, Pd and Co as the reference (units of μ_B, see Table S7) corresponding to the first layer, first to third layers and fourth to sixth layers, respectively. The blue, pink and green symbols respectively denote each layer's average magnetic moment of the Pt_0, Pt_2 and Pt_{16} models, see the data in Table S8. The inserted model structure is the Pt_2 example, detailed model structures see Fig. S1.

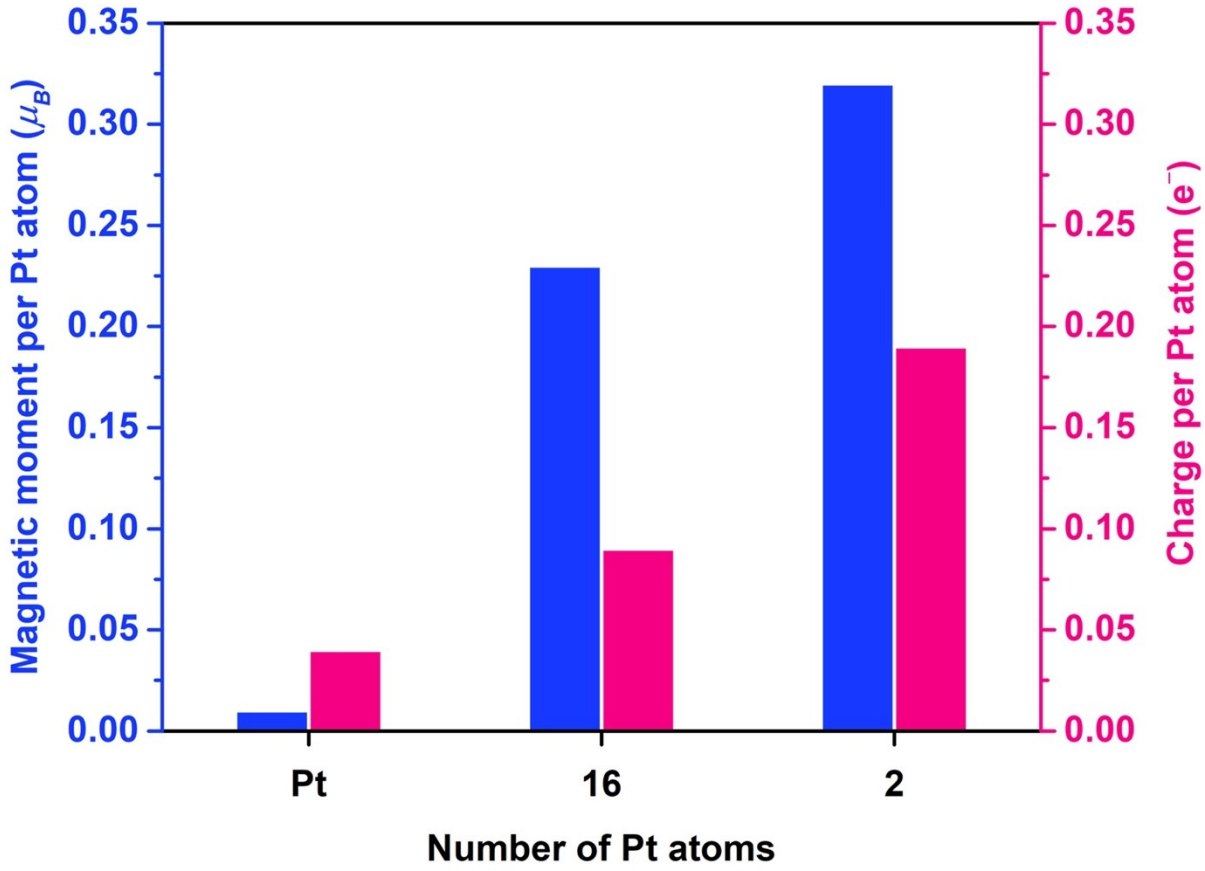

Fig. S6 | Calculated magnetic moment per Pt atom (blue bars) and charge-gain (purple bars) per Pt atom in the first layer of the pure Pt, Pt_{16} and Pt_2 models.

Table S1 | The adsorption energies (E_{ads}, given in eV) of O_2, O^{ads}, H_2O and OH^- at different adsorption sites corresponding to the different catalyst configurations (Pd (111), Pt_0, Pt_2, Pt_{16}, Pt_{32}, Pt (111)).

	Pd	Pt_0	Pt_2	Pt_{16}	Pt_{32}	Pt
O_2-site / E_{ads}	Pd_2-b −0.75	Pd_2-b −0.80	Pt_2-b −0.90 PtPd-b_1 −0.83 Pt_2-b −0.82	Pt_2-b −0.67	Pt_2-b −0.71	Pt_2-b −0.73
O^{ads}-site / E_{ads}	Pd_3-h −1.15 Pd_3-f −1.34	Pt_3-h −1.14 Pd_3-f −1.32	Pt_2Pd_1-h −1.11 Pt_2Pd_1-f −1.33 Pt_1Pd_2-h −1.08 Pt_1Pd_2-f −1.28 Pd_3-h −1.17 Pd_3-f −1.33	Pt_3-h −0.95 Pt_3-f −1.19	Pt_3-h −0.78 Pt_3-f −1.17	Pt_3-h −0.88 Pt_3-f −1.29
H_2O-site / E_{ads}	Pd_1-t −0.25 Pd_2-b −0.09 Pd_3-f −0.10	Pd_1-t −0.22 Pd_2-b −0.07 Pd_3-f −0.08	Pt_1-t −0.13 Pd_1-t_1 −0.15 Pd_1-t_2 −0.21	Pt_1-t −0.16 Pt_2-b −0.03 Pt_2-f −0.04	Pt_1-t −0.20 Pt_2-b −0.01 Pt_2-f −0.01	Pt_1-t −0.24 Pt_2-b −0.06 Pt_2-f −0.05
OH^--site / E_{ads}	Pd_1-t −2.35 Pd_2-b −2.62 Pd_3-f −2.61	Pt_2-b −2.35 Pd_2-b −2.60 Pd_2-f −2.59	Pt_2-b −2.49 PtPd-b −2.59 Pd_2-b −2.62	Pt_2-t −2.35 Pt_2-b −2.38 Pd_3-f −2.37	Pt_2-t −2.40 Pt_2-b −2.41 Pd_3-f −2.39	Pt_2-t −2.42 Pt_2-b −2.50 Pt_2-f −2.48

Table S2 | Reaction energy barrier (ΔE) of O_2 dissociation (stage I, ΔE^{O-O}) and O^{ads} hydration (stage II, ΔE-O^{ads}/H) of the three possible ORR reaction pathways on the Pt_2 surface model.

ORR Stage	Pt_2-b path	PtPd-b path	Pd_2-b path
I. O_2 dissociation (eV)	0.44	0.36	0.56
II. O^{ads} hydration (eV)	0.10	0.18	0.32

Table S3 | Reverse reaction energy barrier (ΔE^R) of O_2 dissociation (stage I, ΔE^{O-O-R}) and O^{ads} hydration (stage II, ΔE^R-O^{ads}/H) of the three possible ORR reaction pathways on the Pt_2 surface model.

ORR Stage	Pt_2-b path	PtPd-b path	Pd_2-b path
I. O_2 dissociation (eV)	1.63	1.49	1.97
II. O^{ads} hydration (eV)	0.08	0.01	0.03

Table S4 | Reaction energy barrier (ΔE) of the selected O_2 dissociation (ΔE^{O-O}) and O^{ads} hydration (ΔE-O^{ads}/H) pathways on the pure Pd, Pt_0, Pt_2, Pt_{16}, Pt_{32} and pure Pt surface models.

ORR Stage	Pd	Pt_0	Pt_2	Pt_{16}	Pt_{32}	Pt
I. O_2 dissociation (eV)	0.62	0.62	0.44	0.65	0.70	1.04
II. O^{ads} hydration (eV)	0.21	0.16	0.10	0.10	0.01	0.02

Table S5 | Reverse reaction energy barrier (ΔE^{R}) of the selected O_2 dissociation ($\Delta E^{O\text{-}O\text{-}R}$) and O^{ads} hydration (ΔE^{R}-O^{ads}/H) pathways on the pure Pd, Pt_0, Pt_2, Pt_{16}, Pt_{32} and pure Pt surface models.

ORR Stage	Pd	Pt_0	Pt_2	Pt_{16}	Pt_{32}	Pt
I. O_2 dissociation (eV)	1.84	1.88	1.60	1.66	1.42	2.55
II. O^{ads} hydration (eV)	0.08	0.08	0.08	0.06	0.14	0.11

Table S6 | Work function of different surface model systems, including Co, Pd, Co@Pd-Pt_n (n=0, 2, 16 and 32) and Pt.

	Co	Pd	Pt_0	Pt_2	Pt_{16}	Pt_{32}	Pt
Work function (eV)	5.09	5.23	5.27	5.34	6.32	6.36	5.73

Table S7 | The calculated spin magnetic moment of pure Pt, Pd and Co surface models. For comparison, the calculated magnetic moments per atom for bulk Pt, Pd and Co are shown in units of μ_B.

	1st layer	2nd layer	3rd layer	4th layer	5th layer	6th layer	μ_B
Pt	0.00	0.00	0.00	0.00	0.00	0.00	0.00
Pd	0.25	0.38	0.38	0.38	0.38	0.25	0.31
Co	1.73	1.67	1.65	1.66	1.68	1.79	1.67

Table S8 | The calculated magnetization of the Pt_0, Pt_2 and Pt_{16} surface models. For the Pt_2, the "Pt" and "Pd" of the first layer represent the average magnetic moment of the two Pt atoms and the remaining fourteen Pd atoms in this atomic layer, respectively (also applicable to the Pt_0 and Pt_{16}). The other "Pd" and "Co" labels represent the average magnetic moment corresponding to the single atomic layer from top to bottom within the 4×4 supercell, respectively.

	1st layer (Pt)	1st layer (Pd)	2nd layer (Pd)	3rd layer (Pd)	4th layer (Co)	5th layer (Co)	6th layer (Co)
Pt_0	/	0.31	0.31	0.31	1.67	1.67	1.67
Pt_2	0.32	0.28	0.32	0.29	1.80	1.68	1.42
Pt_{16}	0.23	/	0.30	0.27	1.74	1.50	0.98

Table S9 | The core/shell interlayer spacing (given in Å) of 3rd–4th layer from surface to bottom layers in trimetallic Pt_2@Co/Pd models (Δd_{Pt2}), and the corresponding strain values (given in %) relative to Pd(111) or Co(111). The ideal interlayer spacing of of 3rd–4th layer in pure Co(111) and pure Pd(111) are denoted as Δd_{Co} and Δd_{Pd}, respectively.

	Co(111) (Δd_{Co})	Pd(111) (Δd_{Pd})	Pt_2@Co/Pd (Δd_{Pt2})	vertical strain value, type

3^{rd}–4^{th} layer		2.279	2.084	– 8.56%, compressive From $(\Delta d_{Pd} - \Delta d_{Pt2})/\Delta d_{Pd}$
3^{rd}–4^{th} layer	2.016		2.084	+ 3.37%, tensile From $(\Delta d_{Co} - \Delta d_{Pt2})/\Delta d_{Co}$